Pre- and Post-Fire Comparison of Forest Areas in 3D

Devrim Akca, Efstratios Stylianidis, Daniela Poli, Armin Gruen, Orhan Altan, Martin Hofer, Konstantinos Smagas, Victor Sanchez Martin, Andreas Walli, Elisa Jimeno and Alejandro Garcia

Abstract A satellite processing platform for high resolution forest assessment (FORSAT) was developed. It generates the digital surface models (DSMs) of the forest canopy by advanced processing of the very-high resolution (VHR) optical satellite imagery and automatically matches the pre- and post-fire DSMs for 3D change detection. The FORSAT software system can perform the following tasks: pre-processing, point measurement, orientation, quasi-epipolar image generation, image matching, DSM extraction, orthoimage generation, photogrammetric restitution either in mono-plotting mode or in stereo models, 3D surface matching, co-registration, comparison and change detection. It can thoroughly calculate the planimetric and volumetric changes between the epochs. It supports most of the VHR optical imagery commonly used for civil applications. Capabilities of

D. Akca (✉)
Isik University, Istanbul, Turkey
e-mail: akca@isikun.edu.tr

E. Stylianidis
Aristotle University of Thessaloniki, Thessaloniki, Greece
e-mail: sstyl@auth.gr

D. Poli
4DiXplorer AG, Zurich, Switzerland
e-mail: daniela@4dixplorer.com

A. Gruen
ETH Zurich, Switzerland/4DiXplorer AG, Zurich, Switzerland
e-mail: agruen@geod.baug.ethz.ch; agruen@4dixplorer.com

O. Altan
Istanbul Technical University/Ekinoks Surveying Software Engineering Ltd, Istanbul, Turkey
e-mail: oaltan@itu.edu.tr; altan@ekinoks3d.com

M. Hofer · A. Walli
GeoVille Information Systems GmbH, Innsbruck, Austria
e-mail: hofer@geoville.com

A. Walli
e-mail: walli@geoville.com

O. Altan et al. (eds.), *Intelligent Systems for Crisis Management*,
Lecture Notes in Geoinformation and Cartography,
https://doi.org/10.1007/978-3-030-05330-7_11

FORSAT have been tested in two real forest fire cases, where the burned areas are located in Cyprus and Austria. The geometric characteristics of burned forest areas have been identified both in 2D plane and 3D volume dimensions, using pre- and post-fire optical image data from different sensors. The test studies showed that FORSAT is an operational software capable of providing spatial (3D) and temporal (4D) information for monitoring of forest fire areas and sustainable forest management. Beyond the wildfires, it can be used for many other forest information needs.

1 Introduction

Deforestation is one of the major sources of carbon emission which threatens the global climate targets. Several satellites and sensors have been used to monitor deforestation areas. The Advanced Very High Resolution Radiometer (AVHRR) on board the NOAA-series satellites (Di Maio Mantovani and Setzer 1997), JERS-1 (Almeida-Filho et al. 2005), MODIS on-board the NASA EOS satellites (Anderson et al. 2005), ASTER (Haboudane and Bahri 2008), Formosat-2 (Baillarin et al. 2008), PALSAR on-board ALOS (Isoguchi et al. 2009) constitute a small set of examples.

Low to medium resolution level optical images present drawbacks for operation in the moist tropics and in all weather conditions, synthetic aperture radar (SAR) data might be seen as an alternative (Santos et al. 2008; Solberg et al. 2013). Applications of SAR data to map deforestation are generally based on the assumption that undisturbed forests consistently exhibit higher radar backscatter than deforested areas. Depending on the stage of the deforestation process (slashing, burning and terrain clearing), this assumption is not always valid, and deforested areas may display a stronger radar return backscatter than primary forest (Almeida-Filho et al. 2007). Especially, new deforested areas are not unequivocally detected in some cases (Almeida-Filho et al. 2009).

With over 30 years of directly comparable satellite observations, now freely available and new imagery being added to the archive every day, Landsat time

K. Smagas
GeoImaging Ltd, Nicosia, Cyprus
e-mail: kostas@geoimaging.com.cy

V. S. Martin · E. Jimeno · A. Garcia
Ingeniería Y Soluciones Informáticas S.L., Seville, Spain
e-mail: vsanchez@isoin.es

E. Jimeno
e-mail: elisa.jimeno@isoin.es

A. Garcia
e-mail: agarcia@isoin.es

series legacy affords novel opportunities for ecosystem mapping, environmental monitoring and comparative ecology (Pasquarella et al. 2016). It has been used to understand the space-time dynamics of deforestation over large areas, but at moderate resolution (Alves 2002; Ichii et al. 2003; Bodart et al. 2011; Souza et al. 2013).

Measuring the areal extent of deforestation for other than localized areas requires the use of fine resolution satellite data. An accurate determination of deforestation is very difficult to achieve by a random sampling analysis of Landsat or similar resolution data unless a very high percentage of the area to be studied is sampled (Tucker and Townshend 2000). The very high resolution (VHR) satellite imagery is an alternative and effective solution (Mora et al. 2013). Availability and metric capability of the VHR satellite imagery is given in Remondino (2011) and Sefercik et al. (2013).

Conventional forest inventory contains extensive field work to collect data of coverage, specie, height, volume, health, damage, change, deforestation, etc. It is expensive and time consuming (Eva et al. 2010; Koch 2010). Although the traditional forest inventory methods are the most accurate, they are neither agile nor economic. Alternative management strategies are required (Mondal et al. 2010). The Global Forest Watch (GFW) is one of the example of the worldwide responses to this demand, which is an open-source web application to monitor global forests in near real-time (http://www.globalforestwatch.org). It is an initiative of the World Resources Institute (WRI) with partners including Google, Esri and many other academic, non-profit, public and private organizations. The Global Forest Observations Initiative (GFOI) is another international collaboration to support countries to develop their national forest monitoring systems (http://www.gfoi.org/). The satellite data primarily comes from USGS Landsat series, and EU Copernicus Programme ESA Sentinel-1 radar and Sentinel-2 optical series. Japan (JAXA), Brazil (INPE), China (CRESDA), France (CNES), Italy (ASI), Canada (CSA) and Germany (DLR) provides additional contributions.

Deforestation is caused by ever-increasing activities of the growing human population (Pahari and Murai 1999), its density (Svancara et al. 2009) and agricultural colonisation (Millington et al. 2003). Their effects are seen in long terms. On the other hand, the forest fire, which is another main cause of deforestation, is a rapid event whose effects are seen in very short terms (Lee 2008). A rapid, effective and economic way of change detection is required in order to understand the pre- and post-fire changes of forest areas. The VHR satellite imagery which allows stereo and triplet acquisitions at very fine spatial resolutions offers less expensive, faster and more agile remote sensing capacities than the alternative technologies, thereby providing an optimum solution for such change detection tasks. Additional advantages are no overflight permissions needed, an optimum ground coverage capacity versus spatial resolution, and repetition of image acquisitions on a certain area of interest until cloud coverage is free. FORSAT (a satellite processing platform for high resolution forest assessment) is an operational software system designed to fulfil these special requirements in the forestry sector, which was originally a research and development project funded by Eurostars (https://www.eurostars-eureka.eu/) and the European Commission. It is a standalone satellite-based monitoring capacity specifically for 3D forest cover mapping and change detection applications. Moreover, it is a processing platform, where high performance and well-studied methods of the terrestrial and airborne techniques are coupled with the spaceborne VHR image data, to obtain a single source forest information system.

The FORSAT software can generate digital surface models (DSM) of forest canopy in high resolution and accuracy. By comparing pre- and post-fire DSMs, the system allows automatic 3D change detection of forest and non-forest areas along with change both in area and volume dimensions.

In the next section, state-of-the-art methods for forest fire prediction, detection, monitoring and measurement are reviewed. In the third section, the FORSAT methodology is presented with its algorithmic details. Performance of the FORSAT software was tested by executing case studies at two forest fire areas located in Cyprus and Austria. The experimental results have proved that public bodies and private organisations can use the VHR satellite data for many forest information needs. In the fourth section, the results achieved on the test cases are reported and discussed. The final conclusions are given in the fifth section.

2 Forest Fire Prediction, Detection, Monitoring and Measurement

Thanks to the rising public awareness and comprehensive forest protection programs, the global vegetation showed a remarkable greening (+0.28% per year) over browning (−0.14% per year) based on the Moderate Resolution Imaging Spectroradiometer (MODIS) vegetation index data from 2011 to 2015 (Zhang et al. 2017). The forest fire is one of the major threats that attenuate this global greening trend. Human-started fires represent the vast majority of wildfires whose distance from built-up areas becomes closer-and-closer by the time (Mancini et al. 2018).

The susceptibility of forest fires increases with direct human activities, road accessibility, forest fragmentation, habitat loss and similar causes (Mancini et al. 2018; Silva Junior et al. 2018). This list can be extended. All these factors together with meteorological data (Yu et al. 2017), weather variables (Sun and Zhang 2018), surface temperature and water content (Abdollahi et al. 2018) and elevation data (Adelabu et al. 2018) can be appropriately combined to establish forest fire prediction and forecasting models. The fire danger forecast module of the European Forest Fire Information System (EFFIS), is an active web-based system all year around, generates daily maps of 1 to 10 days of forecasted fire danger level using numerical weather predictions (http://effis.jrc.ec.europa.eu/).

Such models support risk assessment and mitigation, decision making and fire management activities (Altan et al. 2013; Nyongesa and Vacik 2018).

Early detection of forest fires is of vital importance as it saves critical times for fire extinguishing activities. The human visualization system is not optimally suited for fire detection. Smoke occlusion heavily limits flame visibility and low flames can be difficult to see. Thermal infrared (TIR) and near-infrared (NIR) sensors mitigate these affects and are widely used for fire detection (Burnett and Wing 2018). The satellite platforms offer wider field-of-view (FOV) at reasonable cost and with flexible operational capabilities. The satellite sensors that are widely used in fire detection are the Advanced Spaceborne Thermal Emission and Reflection Radiometer (ASTER), EO-1 Advanced Land Imager (ALI), Advanced Very High Resolution Radiometer (AVHRR), Moderate Resolution Imaging Spectroradiometer (MODIS), Landsat 7 Enhanced Thematic Mapper Plus (ETM+) and Landsat 8 Operational Land Imager (OLI). All of them are owned by NASA except the AVHRR by NOAA (Camaro et al. 2013).

MODIS offers several data products. Among them, the MODIS Thermal Anomalies/Fire products (https://modis.gsfc.nasa.gov/data/dataprod/) are the most used products to monitor and to detect hotspots and burned areas worldwide (Justice et al. 2002a, b). The product includes fire occurrence (day/night), fire location, the logical criteria used for the fire selection, detection confidence, Fire Radiative Power and numerous other layers describing fire pixel attributes. The product distinguishes between fire, no fire and no observation statuses. The embedded fire detection strategy is based on absolute detection (when the fire strength is sufficient to detect) and on detection relative to its background. An improved fire hotspot detection algorithm was proposed by Giglio et al. (2003) which uses a contextual algorithm exploiting the observations from several MODIS channels. The Fire Information for Resource Management System (FIRMS) is a web application that delivers global MODIS hotspots and fire locations in an easy to use format (http://earthdata.nasa.gov/data/near-real-time-data/firms).

The GOFC/GOLD (Global Observations of Forest and Land Cover Dynamics) is a project to provide a forum for international information exchange, observation and data coordination, and a framework for establishing the necessary long-term monitoring systems. The web site (http://gofc-fire.umd.edu/projects/index.php) lists several active fire detection and monitoring systems.

Numerous fire detection algorithms have been developed using the MODIS fire products (Giglio et al. 2016). The MODIS products are not only used for detecting wildfires but also for tree cover loss caused by illegal clearing, interdict deforestation and other reasons (Wheeler et al. 2018).

The Visible Infrared Imaging Radiometer Suite (VIIRS) aboard the Suomi National Polar–orbiting Partnership (Suomi-NPP) satellites, the Spinning Enhanced Visible and InfraRed Imager (SEVIRI) on board the Meteosat Second Generation (MSG) satellites, the Advanced Baseline Imager (ABI) on board the Geostationary Operational Environmental Satellite-R Series (GOES-R) and the Visible and Infra-Red Radiometer (VIRR) on board the Chinese FengYun-3C satellite are also used for active fire detection (Schroeder et al. 2014; Filizzola 2016; Koltunov et al. 2016; Lin et al. 2018).

Satellite sensors are feasible sources to be used for on-instant (or near real-time) monitoring of forest fires. NASA's Aqua satellite, carrying a MODIS sensor, captured the several parallel fires of California in a single scene on July 29, 2018. More than 85,541 hectares were burned, and eight civilians died. The second-deadliest wildfire in the 21st century, happened in Attica, Greece, in July 2018, was imaged by GeoEye-1 satellite. Ninety-nine people were dead and thousands of homes were destroyed. Planet, a Californian company, operates 130+ PlanetScope Dove, 13 SkySats and 5 RapidEye satellites to monitor the ground in near real-time, which are also frequently used to monitor active forest fires (https://www.planet.com/). USA Wildfires interactive map, which is an ESRI Storymap (https://storymaps.esri.com/stories/usa-wildfires/), shows location, magnitude and status of active fires raging across the United States. It is a good example of internet-based mapping applications which is used for near real-time monitoring of forest fires.

Burn severity metrics are useful indicators to assess the post-fire conditions in terms of forest damage and loss (Navarro et al. 2017). At least two images capturing the pre- and post-fire status are required, which would be SAR (Addison and Oommen 2018), VHR optical (Meng et al. 2017) or medium resolution multispectral (Edwards et al. 2018; Fernandez-Garcia et al. 2018) images. If mapped with appropriate cartographic techniques, the burn severity provides valuable information to forest managers for their restoration efforts in terms of post-fire recovery, regeneration and vegetation succession (Ryu et al. 2018; Vega et al. 2018; Li et al. 2018). The geomatics (geo-spatial) platforms, sensors and techniques offer a wide variety of solutions for rapid mapping of natural hazards including the wildfires (Toschi et al. 2017; Toschi et al. 2018). The primary focus is on the most recent satellites (Colson et al. 2018) and unmanned aerial vehicle (UAV) platforms (GW website 2018). The Global Ecosystem Dynamics Investigation (GEDI), pronounced like "Jedi" of Star Wars fame, will be the first space-borne laser instrument to measure the height, density and structures of forests in high resolution and three dimensions (https://gedi.umd.edu/). The expected launch to the International Space Station (ISS) is in late 2018. Although NASA has other space-borne LiDAR missions such as the ICESat (Ice, Cloud and land Elevation Satellite) and CALIPSO (Cloud-Aerosol Lidar and Infrared Pathfinder Satellite Observation), the GEDI will be the first to provide laser ranging of Earth's forests.

After the forest fire lasts, the burned area should be estimated and mapped in order to derive the canopy cover change (McCarley et al. 2017; Cabral et al. 2018; Garcia-Lazaro et al. 2018; Krasovskii et al. 2018). This is predominantly accomplished with either multi-spectral remote sensing data or through ground-based field sampling plots (McCarley et al. 2017). The main emphasis is given to the performance of several parametric and non-parametric classifiers (Ramo et al. 2018). The temporal dimension of post-fire changes is also attributed by analysing the data in time series (Tian et al. 2018; Mayr et al. 2018). The output is typical 2D map depicting the post-fire effects, since the standard burnt area products deal with area computation, which are usually given in hectare units (Soto-Berelov et al. 2018).

Even though the spatial dimension of forest fire changes is relatively less studied, the burned volume would give much more valuable information than the burned area. Volume computation requires more effort both in data and processing aspects (Cailliez 1992). It is actively used in many scientific studies from static object modelling to dynamic flow measurements (Schanz et al. 2018). Limited number of studies has been performed for the forest (or deforestation) volume computation. In a few number of studies, forest volume is conventionally predicted by interpolation methods (Xu et al. 2018).

The FORSAT methodology follows an alternative approach, in which the pre- and post-fire forest surfaces are modelled by generating DSMs derived from the VHR satellite images. The fire related changes are analysed through the comparison of pre- and post-fire DSMs. This operation is known as DSM of difference (DoD), where cell-by-cell subtraction (or other kind of operations) is performed to calculate the total volumes of change (Cucchiaro et al. 2018). If the image data of several epochs are available, temporal-spatial analysis can also be done as time-series, thus allowing 4D analysis and interpretation capabilities.

3 FORSAT Methodology

The FORSAT software allows processing the satellite imagery and extracting meaningful and quantitative information about forests, such as area and volume measurements of deforestation or regeneration of a forest. The software architecture comprises four building blocks for (1) pre-processing, (2) geo-referencing, (3) DSM generation and (4) 3D co-registration and comparison.

Each block is tightly coupled in a software suite framework. The FORSAT software suite is not a monolithic system, that is, every core module works independently but related to each other at the same time. It uses a graphical user interface (GUI) which eases users to work with the software (Fig. 1).

The entire system is an effective combination of two main tasks. The first one is dedicated to the geometric and radiometric processing of satellite imagery and 2D/3D information extraction, that is: radiometric pre-processing, image and

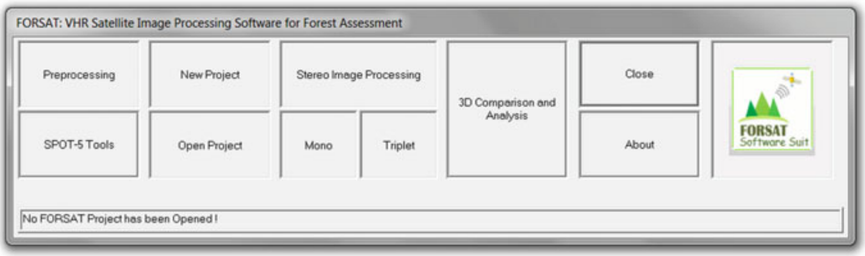

Fig. 1 The graphical user interface of the FORSAT software

ground point measurement and sensor orientation, quasi-epipolar image derivation, image matching, DSM extraction, ortho-rectification, and 3D vector measurement.

This unit supports most of the VHR optical imagery commonly used for civil applications, for example IKONOS, GeoEye-1, WorldView-1/2, SPOT-5/6/7, Pleiades-1A/1B, and it can be easily updated to similar images from future missions.

The second task is dedicated to 3D surface comparison for change detection. It allows the users to import DSMs and digital terrain models (DTMs), to align them using an advanced 3D surface matching technique, and to calculate the 3D volume differences.

The technical approach comprises a bunch of interconnected algorithms whose details are given in Poli (2005), Zhang (2005) and Akca (2007) all of which are the doctoral theses performed at the photogrammetry group of ETH Zurich. Later on, these algorithms were commercialized by 4DiXplorer AG (www.4dixplorer.com), an ETH spin-off company located in Zurich. The FORSAT software is a specialization of these base algorithms to forestry applications, and distributed by 4DiXplorer AG.

3.1 Pre-processing

The VHR satellite images are provided together with their metadata by the vendors. Before applying the algorithms for the geo-referencing of the images, some operations are required in order to prepare the input data. The pre-processing includes both the analysis of the metadata files for the extraction of the required information and the radiometric improvement of the images in order to facilitate the point measurements (Poli 2007).

The performance of the image matching and feature extraction procedures depends on the quality and quantity of information carried out by the images. Compared to the traditional scanned 8-bit/pixel images, digital imagery from linear array sensors has better radiometric performance e.g. higher dynamic range and signal-to-noise ratio. Most of the linear array sensors have the ability to provide high quality digital images. However, some radiometric problems still have to be considered: poor image contrast, the image blur problems mainly caused by CCD line jitter, kappa jitter and motion blur and deficiencies of the lens system, image noise, and radiometric problems caused by the variations in the sensor view angle, the sun angle, shadowing, and the seasonal and the atmospheric conditions. These problems are usually beyond the control of the users. However, they have to be restored as much as possible. In order to reduce the effects of such radiometric problems and optimise the images for subsequent feature extraction and image matching step, the image pre-processing methods have to be employed (Zhang 2005). While the gamma correction, contrast enhancement, histogram equalisation are trivial applications and can be found in many standard image processing software, FORSAT uses the Wallis filter, because it is a specific and powerful

Fig. 2 An image pyramid starting from the original resolution level 0 through the levels 1, 2 and 3 by reducing the image size by factor 3 at each consecutive level

algorithm (Wallis 1976). The filter forces the mean and standard deviation of an image to given target values.

At present, many of the modern matching algorithms are based on the image pyramids (Fig. 2). An image pyramid is a multi-resolution representation of the original image. It is used to speed-up the image matching computation in a coarse-to-fine hierarchical approach while at same time keeping the finest spatial resolution of the final DSM output.

With coarse-to-fine hierarchical strategy based on image pyramid representation, the matches obtained at a coarse resolution are used to guide and limit the search space for the matching of finer-resolution features. The usual way is to start matching at a low resolution pyramid level, where the influence of image noise is reduced and coarse approximate values are sufficient to stay within the pull-in range of the matching procedure. In addition, the regions of interest for correspondence analysis in levels of higher resolution can be found in the low resolution images at low cost because irrelevant details are no longer available there. The computations are usually performed successively on each level of the hierarchy using the results of the higher level as approximate information (Ackermann and Hahn 1991; Zhang and Gruen 2006). The FORSAT software generates the image pyramids at the end of the pre-processing step, starting from the original resolution images. Each pyramid level is generated by multiplying a generating kernel and reduces the resolution by factor 3.

3.2 Geo-referencing

The FORSAT software uses the rational function model (RFM), a well-known non-rigorous (generalised) orientation method based on the rational polynomials functions. A RFM is the ratio of two polynomials derived from the rigorous sensor model and the corresponding terrain information, which does not reveal the sensor parameters explicitly. In most cases, the VHR satellite images are supplied with only rational polynomials coefficients (RPCs) instead of rigorous sensor model parameters.

The RFM is computed based on a rigorous sensor model (Fig. 3). With the given parameters of the rigorous model and by projecting evenly distributed image points into the object space, multiple-layer 3D object points can be computed and used as virtual (fictitious) control points. The control points are created based on the full extent of the image and the range of elevation variation in the object space. The entire range of elevation variation is sliced into several layers. Then, the RPCs are calculated by a least squares adjustment with these virtual control points (Tao and Hu 2001).

Grodecki and Dial (2003) proposed a block adjustment method for the VHR satellite imagery where the geo-referencing accuracy of the RFM is improved by use of a few numbers of control points. This RPC block adjustment method was implemented in the FORSAT software. It can run for stereo, triplet and block image configurations.

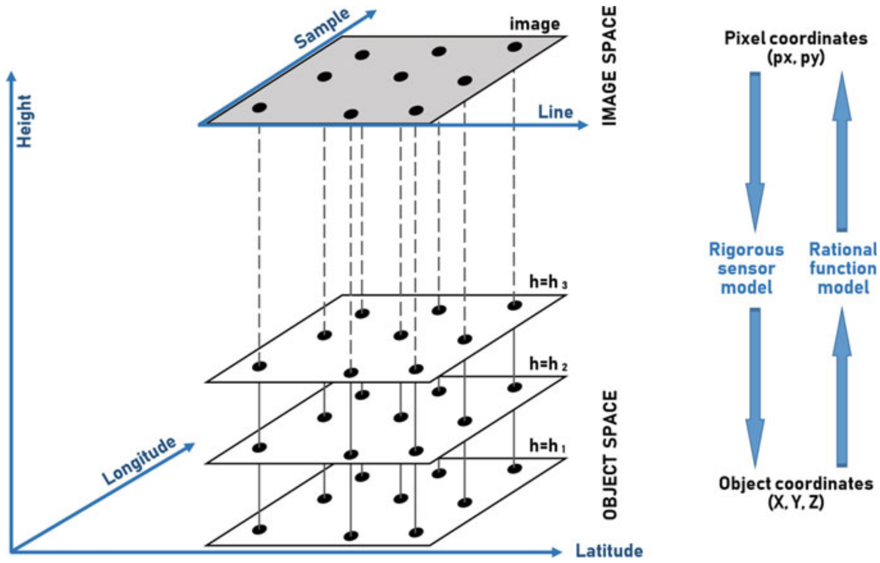

Fig. 3 The RPC computation

3.3 DSM Generation

The automated DSM generation was performed using a modified version of the multiple primitive multi-image matching (MPIM) method introduced by Zhang and Gruen (2004), Zhang (2005) and Zhang and Gruen (2006). In order to achieve successful and reliable results, the method matches a dense pattern of features with an appropriate matching strategy, making use of all available and explicit knowledge, concerning sensor model, network structure, image content and geometrical constraints such as the epipolar geometry constraint. The approach combines area-based matching (ABM) and feature-based matching (FBM), matching parameter self-tuning, generation of more redundant matches and a coarse-to-fine hierarchical matching strategy (Zhang et al. 2006; Baltsavias et al. 2007). The workflow is given schematically in Fig. 4.

After the pre-processing of the original images and production of the image pyramids, the area based and the feature based matching methods are run in parallel. Starting from the low-density features on the images with the low resolution, the matching procedure progressively approaches finally on the original resolution images. Since all the matching procedures are based on the concept of multi-image matching (two-fold and three-fold images) guided from the object space, any number of images could be processed simultaneously. The triangulated irregular network (TIN) is reconstructed from the matched features on each level of the

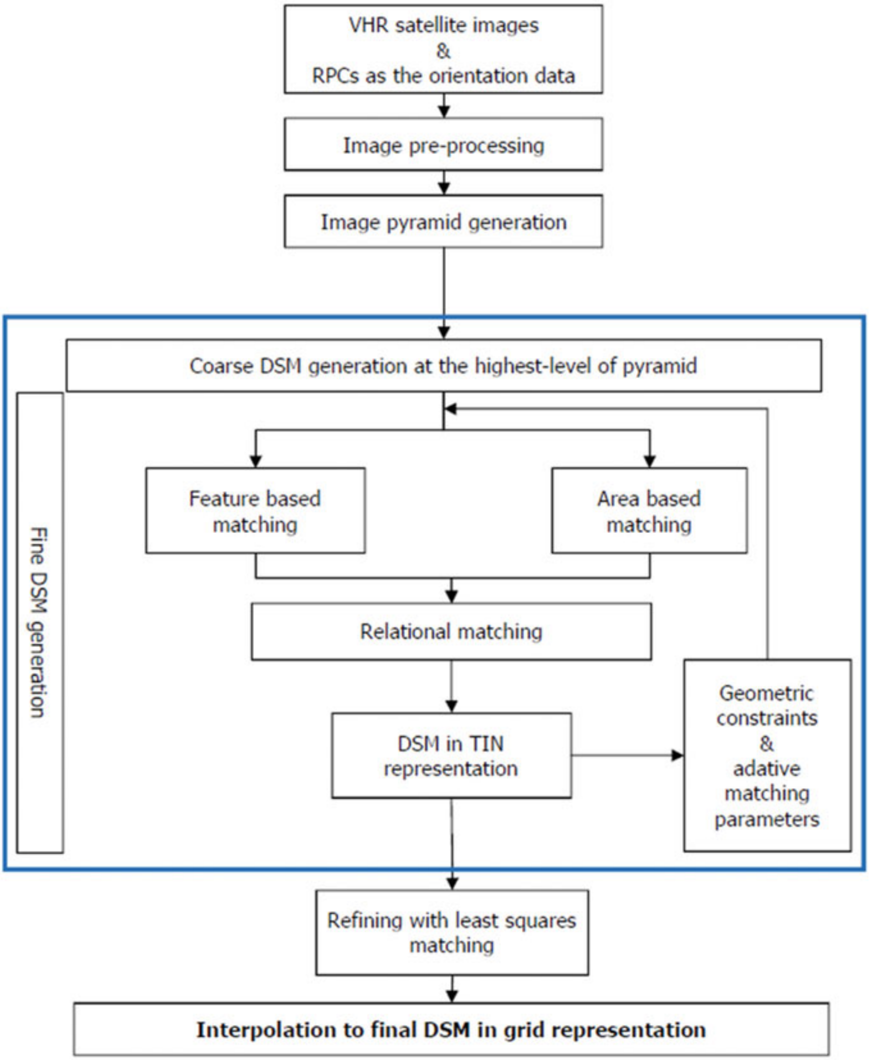

Fig. 4 Automated DSM generation in the FORSAT software

pyramid using the Delaunay triangulation method, which in turn is used in the subsequent pyramid level for the approximations and adaptively computation of the matching parameters. Finally, the least squares matching methods are used to achieve more precise matches for all the features and to identify some false matches.

The entire system consists of three mutually connected sub-systems: the image pre-processing module, the MPIM module and the refined matching module. The image pre-processing module is used to reduce the effects of the radiometric problems and optimise the images for subsequent feature extraction and image matching procedure. A combined matching process (point matching, edge matching and relational matching processes) goes through all the image pyramid levels in the MPIM module and generates good enough approximations for the refined matching module. In the final refined matching module, the least squares matching methods are performed only on the original resolution images to achieve sub-pixel accuracy for all matched features obtained in the MPIM module (Zhang 2005).

3.4 3D Co-registration and Comparison

The co-registration is crucially needed wherever spatially related data sets, described as surfaces, have to be aligned to each other for comparison. Examples can be found in medicine, computer graphics, animation, cartography, virtual reality, industrial inspection and quality control, change detection, spatial data fusion, cultural heritage, photogrammetry, etc. Since DSMs represent the object surface, the problem can be defined as a surface co-registration problem. There have been some studies on the co-registration of DSMs for control information and for change detection tasks. This work is known as the digital elevation model (DEM) matching (Ebner et al. 1988; Rosenholm and Torlegard 1988; Mitchell and Chadwick 1999). This method basically estimates the 3D similarity transformation parameters between two DEM patches, minimising the sum of the squares of the elevation differences (1D along the z-axes). The 1D elevation differences may not truly represent the surface-to-surface distance where terrain is complex with steep changes and undulations.

For quality evaluation of DSMs, often a reference DSM is interpolated in the DSM to be checked. This approach is suboptimal (Gruen et al. 2004; Akca et al. 2016), since:

(1) at surface discontinuities surface modelling errors may lead to large height differences although the measurements are correct (Fig. 5a) and
(2) if the reference frames of the two DSMs differ (e.g. shifts and tilts), then again large differences occur, especially at discontinuities although the heights may be correct (Fig. 5c).

These shortcomings can be overcome by employing the approach where the shortest 3D (Euclidean) distance between each reference point and the produced DSM is used (Gruen and Akca 2005; Akca 2010; Akca et al. 2010). See Fig. 5b and Fig. 5d. Although the co-registration of surfaces is a very actively working area in many disciplines, we notice that a contribution that responds favourably to the following aspects is needed:

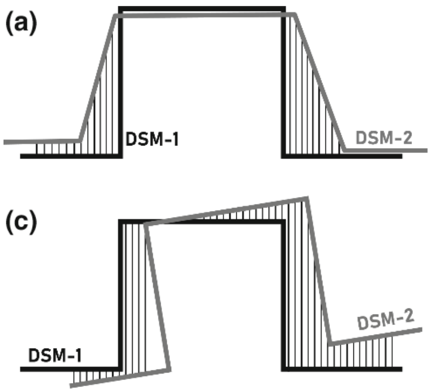

Fig. 5 The sub-optimality of 1D height differences **a** and **c** with respect to the 3D spatial distances **b** and **d** in case of surface modelling errors and reference frame differences (translation and rotation), respectively

(1) co-registration capability with higher order spatial transformation models,
(2) co-registration and comparison of full 3D surfaces (as opposed to 2.5D),
(3) a rigorous mathematical formulation for high accuracy demands,
(4) a flexible model for further algorithmic extensions,
(5) mechanisms and statistical tools for internal quality control, and
(6) capability of matching of data sets in different quality and resolution.

As a consequence, a fully satisfying general solution was implemented in the FORSAT software. We opted for the least squares 3D surface matching (LS3D) method (Gruen and Akca 2005; Akca 2007, 2010). The LS3D method is a rigorous algorithm for the matching of overlapping 3D surfaces and/or point clouds. It estimates the transformation parameters of one or more fully 3D surfaces with respect to a template surface, using the generalised Gauss–Markov model, minimising the sum of the squares of the Euclidean distances between the surfaces. This formulation gives the opportunity to match arbitrarily oriented 3D surfaces, without using explicit tie points. It is a powerful method whose accuracy and precision potential is directly dependent on the quality of the input data. Details of the procedure can be found in Akca and Gruen (2005; 2007). Several applications ranging from 3D modelling (Akca et al. 2006, 2007; Akca 2012) to geomorphology (Akca and Seybold 2016) showed the benefits of the method. The 3D co-registration and comparison module of the FORSAT software is a specialised implementation of the LS3D method.

3.5 Change Detection

Pre- and post-fire DSMs are matched with the co-registration module of the FORSAT software. Once the DSM pair is aligned and overlaid, the two surfaces form many interconnected or separated 3D manifolds (shapes). At each grid cell location, the surface elements are compared and the grid cell is assigned to any of those three states: decrease, no change and increase. Since the grid cell dimensions and surface-to-surface distances are known, the area and volume values are computed by summation the information of all grid cells.

Any spatial deviation larger than ±3 m between the DSMs is regarded as a "change" (fire induced decrease or vegetation growth based increase). This value is the mean a priori accuracy of the used DSMs according to our internal tests with VHR satellite images. The mean DSM generation accuracy of the FORSAT system is about 2–3 times of the ground sampling distance (GSD) of the used imagery. The spatial deviations less than ±3 m are labelled as "no change" class.

The gross errors due to image matching, triangulation and reconstruction problems produce abrupt changes on the DSM surface. Any spatial deviation larger than ±20 m are regarded as the gross error, excluded from the computation, and labelled as "no data". Although they are excluded in the computations, they are kept in the visualizations.

The selection of the threshold numbers as less than or greater than ±3 and ±20 m will accordingly change the ratio of Type-I and II errors. They can be tuned depending on the data type.

3.6 Error Assessment

Three classes "decrease in height", "no change" and "increase in height" are identified in the change detection step. In each test site, externally derived ground truth in the form of check points or polygons are used to perform the error assessment.

A sample point (or polygon) is classified as a true positive (TP), if the detection result corresponds to the reference data. A false positive (FP) error is a false detection where the detection result does not conform to the reference data (Shufelt 1999; McKeown et al. 2000). It is also known as Type-I error or commission error. A false negative (FN) error is a missed detection where an actual class in the reference data is omitted in the detection. It is also known as Type-II error or omission error.

Three commonly used metrics, the correctness, completeness and quality (Heipke et al. 1997; Rutzinger et al. 2009), are used for the evaluation of the results.

Correctness is the percentage of truly detected classes in the sample points, also referred to as users' accuracy (Foody 2002). It is relevant to the FP errors.

$$Correctness_i = (TP)_i / \left[(TP)_i + \sum (FP)_j \right] \tag{1}$$

Completeness is the percentage of truly detected classes in the reference points, also referred to producers' accuracy (Foody 2002). It is relevant to the FN errors.

$$Completeness_i = (TP)_i / \left[(TP)_i + \sum (FN)_j \right] \tag{2}$$

Quality is the overall accuracy which takes into account both the correctness and completeness, also referred to percentage correct (Foody 2002).

$$Quality = \sum (TP)_i / \left[\sum (TP)_i + \sum (FP)_{ij} + \sum (FN)_{ij} \right] \tag{3}$$

The correctness and completeness metrics are computed for each of those three classes, individually. Quality is a single metric for the entire test site, given in the cells located at lower right corners of Tables 1 and 2.

Table 1 Confusion matrix of the Cyprus test site

		Ref.	Ref.	Ref.		
		Decrease	No change	Increase	Row $\sum$	Correct. (%)
Det.	Decrease	40	44	1	85	47.1
Det.	No change	14	83	3	100	83.0
Det.	Increase	1	5	9	15	60.0
	Column $\sum$	55	132	13	200	
	Complet.	72.7%	62.9%	69.2%		66.0

Ref. Reference data, *Det.* Detection data, *Row* $\sum$ Row total, *Column* $\sum$ Column total

Table 2 Confusion matrix of the Austria test site

		Ref.	Ref.	Ref.		
		Decrease	No change	Increase	Row $\sum$	Correct. (%)
Det.	Decrease	19	1	0	20	95.0
Det.	No change	5	92	3	100	92.0
Det.	Increase	0	57	23	80	28.8
	Column $\sum$	24	150	26	200	
	Complet.	79.2%	61.3%	88.5%		67.0

Ref. Reference data, *Det.* Detection data, *Row* $\sum$ Row total, *Column* $\sum$ Column total

4 Experimental Results

4.1 Cyprus Test Site

The climate of Cyprus is characterised by mild and rain-laden winters as well as dry and hot summers. Due to its climate conditions it is predestined for the breakout of forest fires. The high risk for forest ecosystems is also boosted through human interventions. The forest fire of Saittas, raged in 2007, was defined as a test site. The reason for this decision was the disastrous impact of the fire to the local vegetation which is still visible despite the long period of years between the event and image acquisition. The area of interest (AOI) covers an area of about 45 km^2 and includes the city of Pelentri in the Limassol district. There was an Ikonos stereo pair from October 2001 available which was used for the calculation of the pre-fire DSM. For the generation of the post-fire DSM a Pléiades stereo pair acquired in July 2014 was used.

The historic DSM (Fig. 6a) and the recent DSM (Fig. 6b) were generated using the FORSAT software. The both DSMs have a resolution of 2.0 m.

The change analysis was performed with "3D Comparison and Analysis" module of the FORSAT software. The effect of the forest fire of year 2007 can be seen in the west part of the change map (see the largest blue circle in Fig. 7 and enlarged 3D view in Fig. 8a). Furthermore, there are smaller burned areas near Pelentri in the north-east of the AOI (see the blue circle in the north-east of Fig. 7 and enlarged view in Fig. 8b). The decreased forest areas in the south-east of the AOI are man-made changes (Fig. 8c).

Figure 9 visualises the percentage of fire-affected vegetation cover in the AOI. It can be seen that conifer forest with nearly 70% is the most affected vegetation by the forest fire in 2007, followed by bushes and shrubs with 9.5% and tree cultivations with 9.2%.

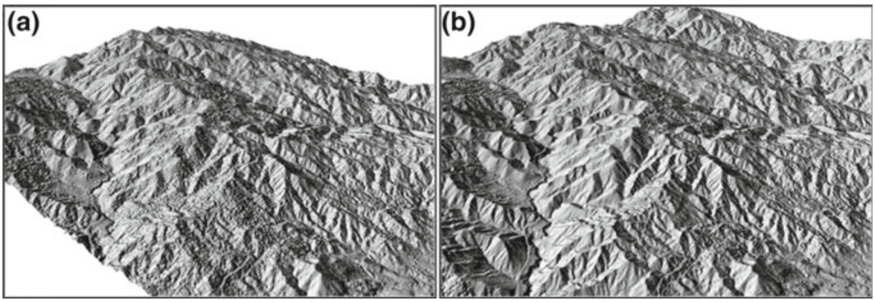

Fig. 6 **a** Ikonos DSM of October 2001, **b** Pléiades DSM of July 2014

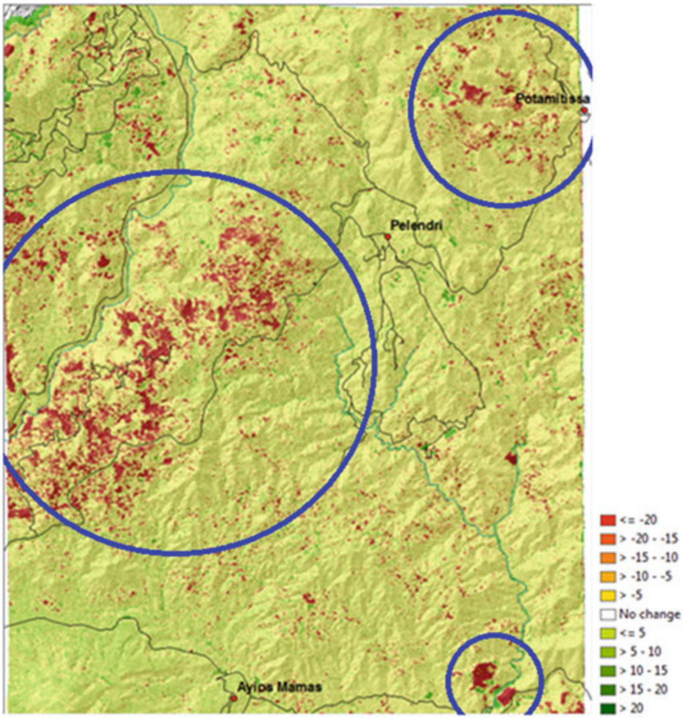

Fig. 7 Change map between pre-fire DSM and post-fire DSM in Cyprus

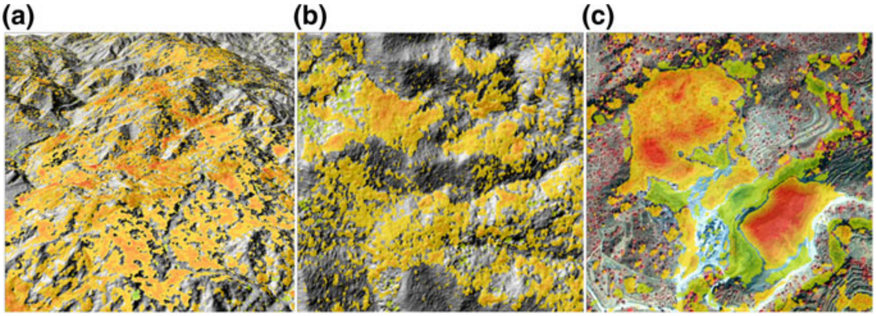

Fig. 8 Zoom into Fig. 7 **a** 3D view of the largest circle region in the centre, **b** the north-east circle region, **c** the south-east small circle region

Figure 10 shows that more than half (54.6%) of the broadleaved forest area, 47.5% of conifer forest and more than a third (36.0%) of the undefined (forest) area were affected by the decrease in height. We noticed that the forest has still not recovered from the fire in 2007.

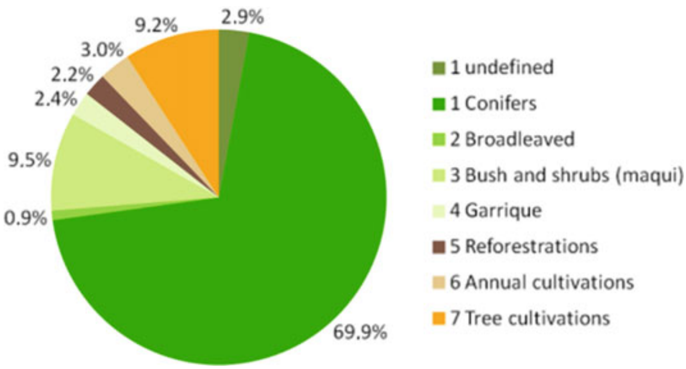

Fig. 9 Percentage of fire-affected vegetation cover in the area of interest

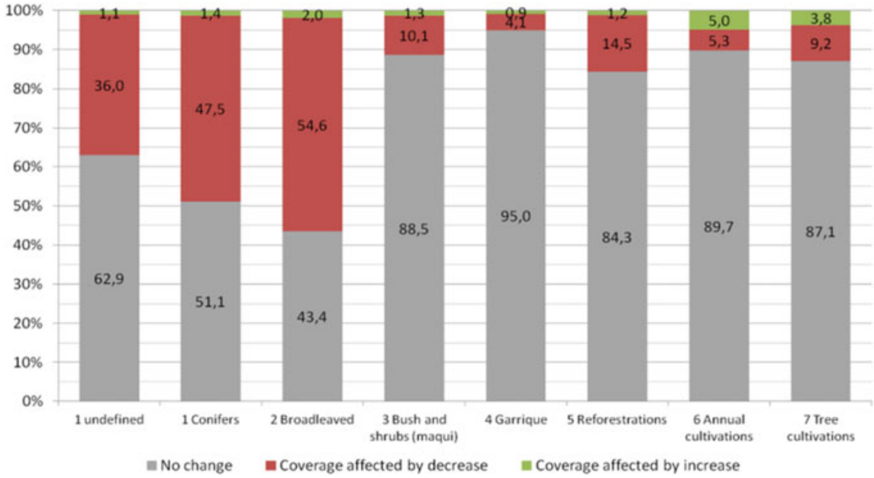

Fig. 10 Change in area (percentage) of fire effected forest vegetation

Figure 11 visualizes the change in volume in fire-affected vegetation cover based on comparison of the DSMs of 2001 and 2014. It illustrates that there is a large decrease (approx. 13 million m^3) of conifer forest. However, this class has also the highest volume increase (365,892 m^3), but it has to be noted that conifer forest cover almost 70% of the whole fire-affected area. Other land cover classes with a volume decrease of nearly 200,000 m^3 and more are undefined forest, broadleaved forest, tree cultivations as well as bush and shrubs (maqui). Besides conifer forest only tree cultivations have a volume increase of more than 100,000 m^3. An interesting fact is that the land cover class annual cultivations decreases the area, but increases the volume in total.

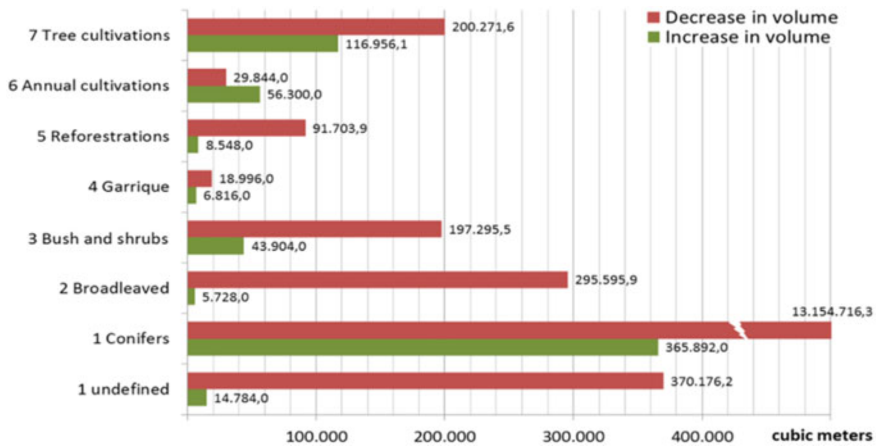

Fig. 11 Change in volume (m3) of fire effected forest vegetation

Fig. 12 Forest fire near Absam, Tyrol, Austria

In order to perform the error assessment, 85, 100 and 15 samples were randomly selected in the detected “decrease in height”, “no change” and “increase in height” classes, respectively. Their actual states were manually investigated on the available aerial and satellite images. The results are presented in a confusion matrix (Table 1). The overall accuracy is 66.0%. There is a tendency towards overestimation of both of the change classes, whilst the “no change” class is underestimated. The “no change” class interferes with the both change classes. This is because of the image matching errors and modelling problems especially at the abrupt surface discontinuities, shadow and cloud coverages. This fact is especially significant in the “decrease in height” class in which 44 FPs were detected mistakenly, although they belong to the “no change” class in reality.

4.2 Austria Test Site

Monitoring of forest areas in terms of quantifying changes over time is a crucial topic in Austria. Strong winds cannot only cause direct damages, but also lead to threats concerning the break out and spreading of forest fires. Fires are great dangers for forests and subsequently for humans as the forests have a protection function for inhabited areas regarding other natural hazards like avalanches, landslides or rock falls. Due to the forest fire event near Absam in Tyrol (Austria), which started on 20-th of March 2014 and raged about two days, the corresponding burned area was selected as a test site (Fig. 12).

The AOI covers about 62 km^2 and includes the burned area from the aforementioned forest fire as well as the eastern suburbs of Innsbruck. Hence, the test site includes a variety of landscapes like mountains, dense urbanised areas surrounded by intensive agriculture as well as rural areas.

The pre-fire data, which dates back to 2006/2007, is a 1.0 m resolution DSM derived from an airborne LiDAR flight (Fig. 13a). A set of Pléiades triplet images was acquired in June 2014 and used to represent the post-fire situation. The Pléiades triplet was processed using the FORSAT software and a 1.0 m resampled DSM was generated (Fig. 13b).

The optical instrument of Pléiades has 70 cm resolution and offers three-fold images of the same scene from the along track trajectory of the platform. The three rays of the same object point increase the system redundancy, and so also the reliability. The LiDAR DSM and Pléiades DSM were co-registered and compared using the LS3D algorithm of the FORSAT software. The result of the 3D change analysis is given in Fig. 14.

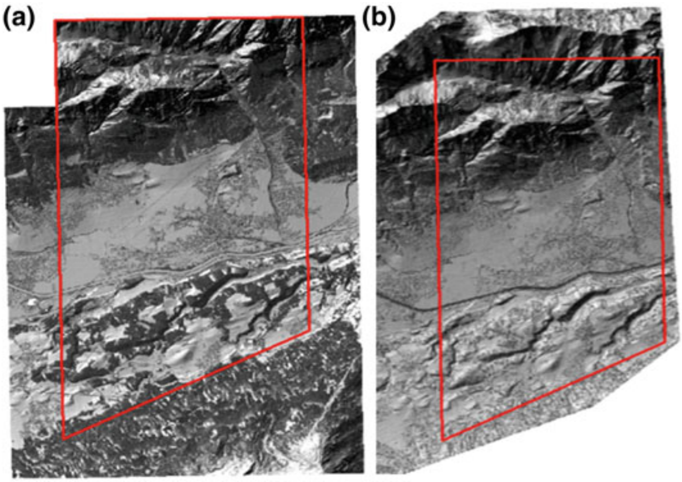

Fig. 13 **a** Historical LiDAR DSM of 2006/2007, **b** recent Pléiades DSM of 2014

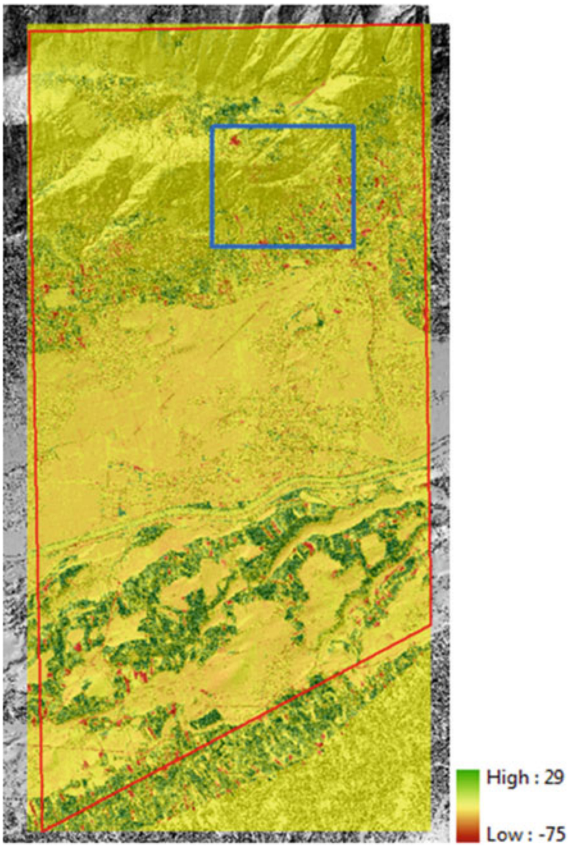

Fig. 14 The 3D Change analysis. Red colour deforestation and green for growth of the vegetation

The occasional clear-cuts and storm damages in the north and the vegetation growth in the south are dominating patterns. The enlarged view of the forest fire, delineated with the blue rectangle, is given in Fig. 15a. The dark green region in the centre of the false colour composite image (Fig. 15b) is the fire affected area, which is shown in orange colour in its change DSM counterpart (Fig. 15a). The fire burned area was dominated by shrubs (proportionally shorter than trees) according to the reports of the Forest Department. This is the reason why the burned areas are not as dominant as the deforestation areas due to clear-cuts or storms such as the red plots in the upper left and lower right parts of Fig. 15a.

There are three classes in the test area: timber forest, shrubs and clear-cuts (Fig. 16). Timber forest is the dominating type with 81.3% coverage.

The forest map showing the boundaries of these three classes is obtained in vector format and overlaid with the change results given in Fig. 14. Thus, areal extends of change of each individual class are computed and given as percentage in Fig. 17.

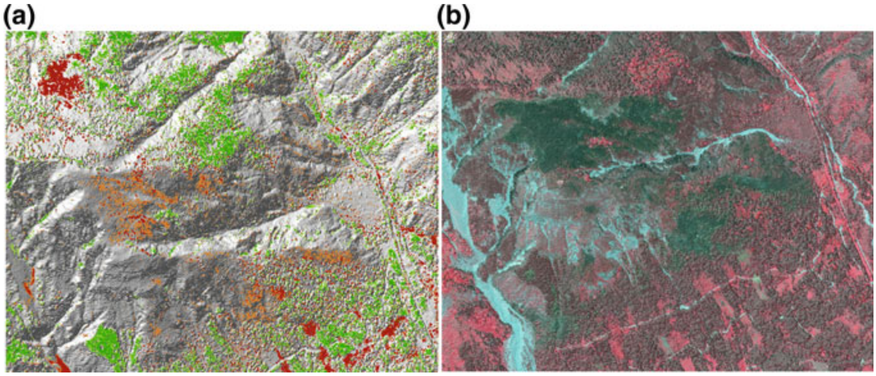

Fig. 15 **a** Enlarged view of the fire area which is shown as a blue rectangle in Fig. 14, **b** Pléiades (in June 2014) false colour composite of the same extend

Fig. 16 Percentage of forest map classes in the area of interest

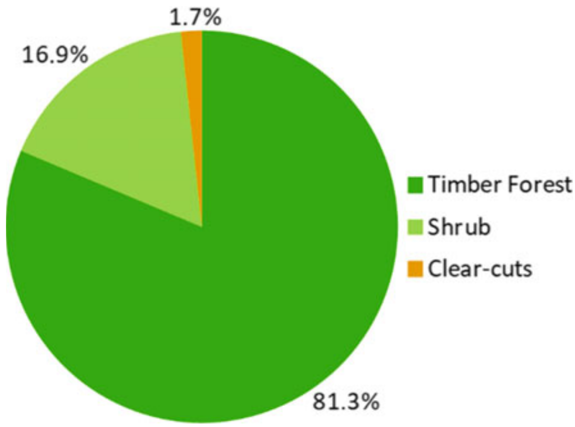

In spite of the forest fire, changes of shrubs are minor, and 99.1% area of the shrubs coverage remained unchanged. 17.5% area of the timber forest class increases in height, which is clearly visible as growth of the vegetation in the southern part of the test area (below green areas in Fig. 14).

The results of the volumetric comparison (Fig. 18) show that the trend is in the same direction with the area comparison, but the magnitude is overwhelmingly nonlinear. The timber forest class gained 17.7 million m^3 volume of stock whereas it lost 7.2 million m^3 due to deforestation. A detailed analysis of the burnt area, visualised in Fig. 15, shows a loss of volume caused by the fire in March 2014 of 41,800 m^3 shrubs and 40,100 m^3 timber forest.

20, 100 and 80 sample points to be used in the error assessment were randomly selected in the detected “decrease in height”, “no change” and “increase in height”

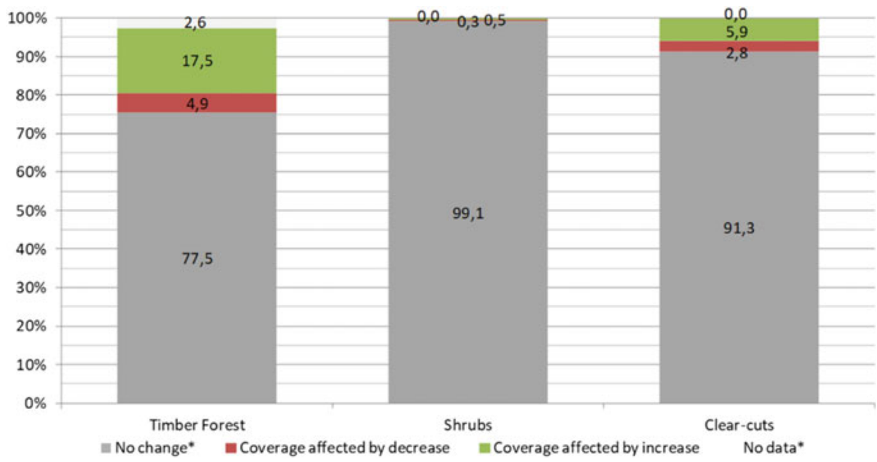

Fig. 17 Change in area (percentage) of each vegetation type

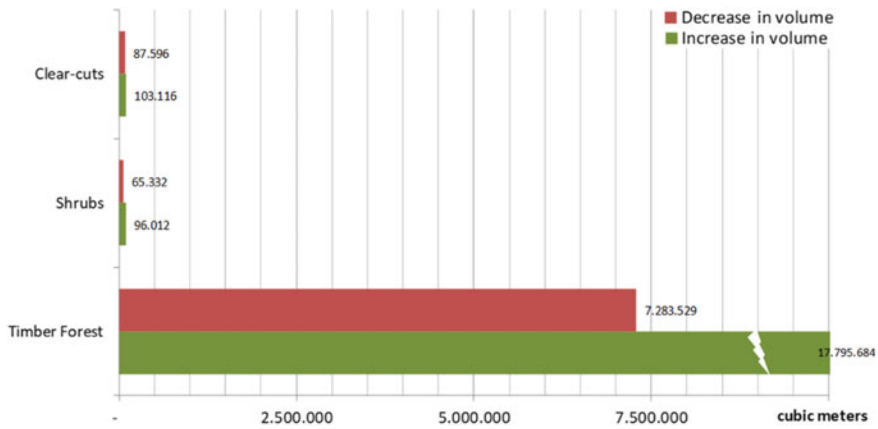

Fig. 18 Change in volume (m3) of each vegetation type

classes, respectively. Their actual states were manually investigated on the available historic orthophotos and actual satellite images. The results are presented in Table 2.

"Decrease in height" class is successfully detected in terms of both the correctness and completeness metrics. "Increase in height" class has the worst FP rate as 100%–28.8% = 71.2%, in contrast to the previous Cyprus test site. "Decrease" and "increase" in height classes do not significantly interfere to each other. "No change" class has the largest FN rate as 38.7%. The discrimination problems between the "no change" and "increase in height" classes degrade the overall accuracy, which is 67.0%.

5 Conclusions

Forest administrations give special attention to forest fires where post-disaster loss can rarely be gauged in a quick and economic way unless an appropriate technology is adopted. Determination of planimetric and volumetric changes between pre- and post-fire stages is in high demand. The FORSAT software was developed to meet the relevant demands. It is capable of providing spatial information for rapid monitoring of forest areas. The basic input data is the VHR satellite imagery. The software consists of mutually linked modules which are pre-processing, geo-referencing, DSM generation, and 3D comparison and analysis.

The pilot application studies demonstrate the capability of the FORSAT software especially for change analysis of the forest burnt areas. Special attention was paid to use combinations of different input data like stereo and triplet image data from different satellites as well as LIDAR point clouds. The results of the applications show the high potential of optical images from VHR satellite sensors for DSM generation on forest covers and that the FORSAT software is a powerful tool to extract value-added products related to forest and beyond. It provides an innovative approach by detecting changes from DEMs of different dates.

The results of FORSAT provide single source, flexible forest information solutions with a very competitive price versus quality ratio, allowing for new market entry in the forest sector. It can be used for various service applications related to forest as well as other topics.

References

Abdollahi M, Islam T, Gupta A, Hassan QK (2018) An advanced forest fire danger forecasting system: integration of remote sensing and historical sources of ignition data. Remote Sens 10:923. https://doi.org/10.3390/rs10060923

Ackermann F, Hahn M (1991) Image pyramids for digital photogrammetry. In: Ebner H, Fritsch D, Heipke C (eds) Digital photogrammetric systems. Wichmann, Karlsruhe, pp 43–58

Addison P, Oommen T (2018) Utilizing satellite radar remote sensing for burn severity estimation. Int J Appl Earth Obs Geoinf 73:292–299

Adelabu SA, Adepoju KA, Mofokeng OD (2018) Estimation of fire potential index in mountainous protected region using remote sensing. Geocarto International. https://doi.org/10.1080/10106049.2018.1499818

Akca D, Gruen A (2005) Recent advances in least squares 3D surface matching. In: Gruen A, Kahmen H (eds) Proceedings of the optical 3-D measurement techniques VII, Vienna, Austria, 3–5 October 2005, vol. II, pp 197–206

Akca D, Gruen A, Alkis Z, Demir N, Breuckmann B, Erduyan I, Nadir E (2006) 3D modeling of the Weary Herakles statue with a coded structured light system. Int Arch Photogramm Remote Sens Spat Inf Sci 36(5):14–19

Akca D (2007) Least Squares 3D surface matching. Ph.D. thesis, Institute of Geodesy and Photogrammetry, ETH Zurich, Switzerland, Mitteilungen Nr. 92, p 78. https://doi.org/10.3929/ethz-a-005461765

Akca D, Gruen A (2007) Generalized Least Squares multiple 3D surface matching. Int Archives Photogramm Remote Sens Spat Inf Sci 36(3/W52):1–7

Akca D, Remondino F, Novàk D, Hanusch T, Schrotter G, Gruen A (2007) Performance evaluation of a coded structured light system for cultural heritage applications. Proc. of SPIE-IS&T Electronic Imaging, Videometrics IX, San Jose, California, January 29–30. SPIE 6491:64910V-1–12

Akca D (2010) Co-registration of surfaces by 3D Least Squares matching. Photogramm Eng Remote Sens 76(3):307–318

Akca D, Freeman M, Sargent I, Gruen A (2010) Quality assessment of 3D building data. Photogram Rec 25(132):339–355

Akca D (2012) 3D modeling of cultural heritage objects with a structured light system. Mediterr Archaeol Archaeom 12(1):139–152

Akca D, Seybold HJ (2016) Monitoring of a laboratory-scale inland-delta formation using a structured-light system. Photogram Rec 31(154):121–142

Akca D, Stylianidis E, Smagas K, Hofer M, Poli D, Gruen A, Martin VS, Altan O, Walli A, Jimeno E, Garcia A (2016) Volumetric forest change detection through VHR satellite imagery. Int Archives Photogramm Remote Sens Spat Inf Sci 41(B8):1213–1220

Almeida-Filho R, Rosenqvist A, Shimabukuro YE, dos Santos JR (2005) Evaluation and perspectives of using multitemporal L-band SAR data to monitor deforestation in the Brazilian Amazonia. IEEE Geosci Remote Sens Lett 2(4):409–412

Almeida-Filho R, Rosenqvist A, Shimabukuro YE, Silva-Gomez R (2007) Detection deforestation with multitemporal L-band SAR imagery: a case study in western Brazilian Amazonia. Int J Remote Sens 28(6):1383–1390

Almeida-Filho R, Shimabukuro YE, Rosenqvist A, Sanchez GA (2009) Using dual-polarized ALOS PALSAR data for detecting new fronts of deforestation in the Brazilian Amazonia. Int J Remote Sens 30(14):3735–3743

Altan O, Backhaus R, Boccardo P, van Manen N, Tonolo FG, Trinder J, Zlatanova S (2013). The value of geoinformation for disaster and risk management (VALID), Joint Board of Geospatial Information Society (JB GIS), Copenhagen, ISBN 97887-90907-88-4

Alves DS (2002) Space-time dynamics of deforestation in Brazilian Amazonia. Int J Remote Sens 23(14):2903–2908

Anderson LO, Shimabukuro YE, Defries RS, Morton D (2005) Assessment of deforestation in near real time over the Brazilian Amazon using multitemporal fraction images derived from Terra MODIS. IEEE Geosci Remote Sens Lett 2(3):315–318

Baillarin F, Souza C, Gonzales G (2008) Use of Formosat-2 satellite imagery to detect near real time deforestation in Amazonia. IEEE International Geoscience & Remote Sensing Symposium (IGARSS'2008). https://doi.org/10.1109/IGARSS.2008.4779481

Baltsavias E, Kocaman S, Akca D, Wolff K (2007) Geometric and radiometric investigations of Cartosat-1 Data. ISPRS Workshop on high resolution earth imaging for geospatial information, Hannover, Germany, 29 May–1 June 2007

Bodart C, Eva H, Beuchle R et al (2011) Pre-processing of a sample of multi-scene and multi-date Landsat imagery used to monitor forest cover changes over the tropics. ISPRS J Photogramm Remote Sens 66:555–563

Burnett JD, Wing MG (2018) A low-cost near-infrared digital camera for fire detection and monitoring. Int J Remote Sens 39(3):741–753

Cabral AIR, Silva S, Silva PC, Vanneschi L, Vasconcelos MJ (2018) Burned are estimations derived from Landsat ETM+ and OLI data: comparing Genetic Programming with Maximum Likelihood and classification and regression trees. ISPRS J Photogramm Remote Sens 142:94–105

Cailliez F (1992) Forest volume estimation and yield prediction. FAO For Paper 22(1):98

Camaro W, Steffenino S, Vigna R (2013) Fire risk mapping and fire detection and monitoring. In: The value of Geoinformation for disaster and risk management (VALID), joint board of geospatial information society (JB GIS), Copenhagen, ISBN 97887-90907-88-4

Colson D, Petropoulos GP, Ferentinos KP (2018) Exploring the potential of Sentinels-1 & 2 of the Copernicus Mission in support of rapid and cost-effective wildfire assessment. Int J Appl Earth Obs Geoinf 73:262–276

Cucchiaro S, Cavalli M, Vericat D, Crema S, Llena M, Beinat A, Marchi L, Cazorzi F (2018) Monitoring topographic changes through 4D-structure-from-motion photogrammetry: Application to a debris-flow channel. Environ Earth Sci 77:632. https://doi.org/10.1007/s12665-018-7817-4

Di Maio Mantovani AC, Setzer AW (1997) Deforestation detection in the Amazon with an AVHRR-based system. Int J Remote Sens 18(2):273–286

Ebner H, Strunz G (1988) Combined point determination using digital terrain models as control information. Int Archives Photogramm Remote Sens 27(B11/3):578–587

Edwards AC, Russell-Smith J, Maier SW (2018) A comparison and validation of satellite-derived fire severity mapping techniques in fire prone north Australian savannas: extreme fires and tree stem mortality. Remote Sens Environ 206:287–299

Eva H, Carboni S et al (2010) Monitoring forest areas from continental to territorial levels using a sample of medium spatial resolution satellite imagery. ISPRS J Photogramm Remote Sens 65:191–197

Fernandez-Garcia V, Santamarta M, Fernandez-Manso A, Quintano C, Marcos E, Calvo L (2018) Burn severity metrics in fire-prone pine ecosystems along a climatic gradient using Landsat imagery. Remote Sens Environ 206:205–217

Filizzola C, Corrado R, Marchese F, Mazzeo G, Paciello R, Pergola N, Tramutoli V (2016) RST-FIRES, an exportable algorithm for early-fire detection and monitoring: description, implementation, and field validation in the case of the MSG-SEVIRI sensor. Remote Sens Environ 186:196–216

Foody GM (2002) Status of land cover classification accuracy assessment. Remote Sens Environ 80:185–201

Garcia-Lazaro JR, Moreno-Ruiz JA, Riano D, Arbelo M (2018) Estimation of burned area in the northeastern Siberian Boreal Forests from a long-term data record (LTDR) 1982-2015 time series. Remote Sens 10:940. https://doi.org/10.3390/rs10060940

Giglio L, Descloitres J, Justice CO, Kaufman YJ (2003) An enhanced contextual fire detection algorithm for MODIS. Remote Sens Environ 87:273–282

Giglio L, Schroeder W, Justice CO (2016) The collection 6 MODIS active fire detection algorithms and fire products. Remote Sens Environ 178:31–41

Grodecki J, Dial G (2003) Block Adjustment of High-Resolution Satellite Images Described by Rational Polynomials. Photogramm Eng Remote Sens 69(1):59–68

Gruen A, Poli D, Zhang L (2004) SPOT-5/HRS stereo images orientation and automated DSM generation. Int Archives Photogramm Remote Sens Spat Inf Sci 35(1):421–432

Gruen A, Akca D (2005) Least squares 3D surface and curve matching. ISPRS J Photogramm Remote Sens 59(3):151–174

GW website (2018) Insitu ScanEagle UAS helps suppress wildfires. https://www.geomatics-world.co.uk/content/news/insitu-scaneagle-uas-helps-suppress-wildfires. Accessed 09 Oct 2018

Haboudane D, Bahri EM (2008) Deforestation detection and monitoring in cedar forests of the Moroccan Middle-Atlas Mountains. IEEE International Geoscience & Remote Sensing Symposium (IGARSS'2007). https://doi.org/10.1109/IGARSS.2007.4423809

Heipke C, Mayer H, Wiedemann C, Jamet O (1997) Evaluation of automatic road extraction. Int Archives Photogramm Remote Sens 32(3–2W3):47–56

Ichii K, Maruyama M, Yamaguchi Y (2003) Multi-temporal analysis of deforestation in Rondonia state in Brazil using Landsat MSS, ETM+ and NOAA AVHRR imagery and its relationship to changes in the local hydrological environment. Int J Remote Sens 24(22):4467–4479

Isoguchi O, Shimada M, Uryu Y (2009) A preliminary study on deforestation monitoring in Sumatra island by PALSAR. IEEE International Geoscience & Remote Sensing Symposium (IGARSS'2009). https://doi.org/10.1109/IGARSS.2009.5417928

Justice CO, Townshend JRG, Vermote EF, Masuoka E, Wolfe RE, Saleous N, Roy DP Morisette JT (2002a) An overview of MODIS Land data processing and product status. Remote Sensing of Environment 83:3–15

Justice CO, Giglio L, Korontzi S, Owens J, Morisette JT, Roy D, Descloitres J, Alleaume S, Petitcolin F, Kaufman Y (2002b) The MODIS fire products. Remote Sens Environ 83:244–262

Koch B (2010) Status and future of laser scanning, synthetic aperture radar and hyperspectral remote sensing data for forest biomass assessment. ISPRS J Photogramm Remote Sens 65:581–590

Krasovskii A, Khabarov N, Pirker J, Kraxner F, Yowargana P, Schepaschenko D, Obersteiner M (2018) Forests 9:437. https://doi.org/10.3390/f9070437

Koltunov A, Ustin SL, Quayle B, Schwind B, Ambrosia VG, Li W (2016) The development and first validation of the GOES Early Fire Detection (GOES-EFD) algorithm. Remote Sens Environ 184:436–453

Lee H (2008) Mapping deforestation and age of evergreen trees by applying a binary coding method to time-series Landsat November images. IEEE Trans Geosci Remote Sens 46 (11):3926–3936

Li X, Zhang H, Yang G, Ding Y, Zhao J (2018) Post-fire vegetation succession and surface energy fluxes derived from remote sensing. Remote Sens 10:1000. https://doi.org/10.3390/rs10071000

Lin Z, Chen F, Niu Z, Li B, Yu B, Jia H, Zhang M (2018) An active fire detection algorithm based on multi-temporal FengYun-3C VIRR data. Remote Sens Environ 211:376–387

Mancini LD, Elia M, Barbati A, Salvati L, Corona P, Lafortezza R, Sanesi G (2018) Are wildfires knocking on the built-up areas door? Forests 9:234. https://doi.org/10.3390/f9050234

Mayr MJ, Vanselow KA, Samimi C (2018) Fire regimes at the arid fringe: A 16-year remote sensing perspective (2000–2016) on the controls of fire activity in Namibia from spatial predictive models. Ecol Ind 91:324–337

McCarley TR, Kolden CA, Vaillant NM, Hudak AT, Smith AMS, Wing BM, Kellogg BS, Kreitler J (2017) Multi-temporal LiDAR and Landsat quantification of fire-induced changes to forest structure. Remote Sens Environ 191:419–432

McKeown DM, Bulwinkle T, Cochran S, Harvey W, McGlone C, Shufelt JA (2000) Performance evaluation for automatic feature extraction. Int Archives Photogramm Remote Sens 33 (B2):379–394

Meng R, Wu J, Schwager KL, Zhao F, Dennison PE, Cook BD, Brewster K, Green TM, Serbin SP (2017) Using high spatial resolution satellite imagery to map forest burn severity across spatial scales in a Pine Barrens ecosystem. Remote Sens Environ 191:95–109

Millington AC, Velez-Liendo XM, Bradley AV (2003) Scale dependence in multitemporal mapping of forest fragmentation in Bolivia: implications for explaining temporal trends in landscape ecology and applications to biodiversity conservation. ISPRS J Photogramm Remote Sens 57:289–299

Mitchell HL, Chadwick RG (1999) Digital photogrammetric concepts applied to surface deformation studies. Geomatica 53(4):405–414

Mondal P, Southworth J (2010) Protection vs. commercial management: spatial and temporal analysis of land cover changes in the tropical forests of Central India. For Ecol Manage 259:1009–1017

Mora B, Wulder MA, White JC, Hobart G (2013) Modeling stand height, volume, and biomass from very high spatial resolution satellite imagery and samples of airborne LiDAR. Remote Sens 5:2308–2326

Navarro G, Caballero I, Silva G, Parra PC, Vazquez A, Caldeira R (2017) Evaluation of forest fire on Madeira Island using Sentinel-2A MSI imagery. Int J Appl Earth Observ Geoinf 58:97–106

Nyongesa KW, Vacik H (2018) Fire management in Mount Kenya: a case study of Gathiuru forest station. Forests 9:481. https://doi.org/10.3390/f9080481

Pahari K, Murai S (1999) Modelling for prediction of global deforestation based on the growth of human population. ISPRS J Photogramm Remote Sens 54:317–324

Pasquarella VJ, Holden CE, Kaufman L, Woodcock CE (2016) From imagery to ecology: leveraging time series of all available Landsat observations to map and monitor ecosystem state & dynamics. Remote Sens Ecol Conserv 2(3):152–170. https://doi.org/10.1002/rse2.24

Poli D (2005) Modelling of Spaceborne Linear Array Sensors. Ph.D. thesis, Institute of Geodesy and Photogrammetry, ETH Zurich, Switzerland, Mitteilungen Nr. 85, p 217

Poli D (2007) A Rigorous Model for Spaceborne Linear Array Sensors. Photogramm Eng Remote Sens 73(2):187–196

Ramo R, Garcia M, Rodriguez D, Chuvieco E (2018) A data mining approach for global burning area mapping. Int J Appl Earth Observ Geoinf 73:39–51

Remondino F (2011) Heritage recording and 3D modelling with photogrammetry and 3D scanning. Remote Sensing 3:1104–1138

Rosenholm D, Torlegard K (1988) Three-dimensional absolute orientation of stereo models using digital elevation models. Photogramm Eng Remote Sens 54(10):1385–1389

Rutzinger M, Rottensteiner F, Pfeifer N (2009) A comparison of evaluation techniques for building extraction from airborne laser scanning. IEEE J Sel Topics Appl Earth Observ Remote Sens 2(1):11–20

Ryu JH, Han KS, Hong S, Park NW, Lee YW, Cho J (2018) Satellite-based evaluation of the post-fire recovery process from the worst forest case in South Korea. Remote Sens 10:918. https://doi.org/10.3390/rs10060918

Santos JR, Mura JC, Paradella WP, Dutra LV, Goncalves FG (2008) Mapping recent deforestation in the Brazilian Amazon using simulated L-band MAPSAR images. Int J Remote Sens 29 (16):4879–4884

Schanz D, Huhn F, Schroeder A (2018) Large-scale volumetric flow measurement of a thermal plume using Lagrangian Particle Tracking (Shake-The-Box). In: Raffel M et al (eds) Particle Image Velocimetry, Springer, 606–610. https://doi.org/10.1007/978-3-319-68852-7_18

Schroeder W, Oliva P, Giglio L, Csiszar IA (2014) The new VIIRS 375 m active fire detection data product: algorithm description and initial assessment. Remote Sens Environ 143:85–96

Sefercik UG, Alkan M, Buyuksalih G, Jacobsen K (2013) Generation and validation of high-resolution DEMs from Worldview-2 stereo data. Photogramm Rec 28(144):362–374

Shufelt JA (1999) Performance evaluation and analysis of monocular building extraction from aerial imagery. IEEE Trans Pattern Anal Mach Intell 21(4):311–326

Silva Junior CHL, Aragao LEOC, Fonseca MG, Almeida CT, Vedovato LB, Anderson LO (2018) Deforestation-induced fragmentation increases forest fire occurrence in Central Brazilian Amazonia. Forests 9:305. https://doi.org/10.3390/f9060305

Solberg S, Astrup R, Weydahl DJ (2013) Detection of forest clear-cuts with Shuttle Radar Topography Mission (SRTM) and Tandem-X InSAR data. Remote Sensing 5:5449–5462

Soto-Berelov M, Jones SD, Clarke E, Reddy S, Gupta V, Felipe MLC (2018) Assessing two large area burnt area products across Australian Southern Forests. Int J Remote Sens 39(3):879–905

Souza CM, Siqueira JV, Sales MH et al (2013) Ten-year Landsat classification of deforestation and forest degradation in the Brazilian Amazon. Remote Sens 5:5493–5513

Sun P, Zhang Y (2018) A probabilistic method predicting forest fire occurrence combining firebrands and the weather-fuel complex in the northern part of the Daxinganling region. China For 9:428. https://doi.org/10.3390/f9070428

Svancara LK, Scott JM, Loveland TR, Pidgorna AB (2009) Assessing the landscape context and conversion risk of protected areas using satellite data products. Remote Sens Environ 113:1357–1369

Tao CV, Hu Y (2001) A Comprehensive Study of the Rational Function Model for Photogrammetric Processing. Photogramm Eng Remote Sens 66(12):1477–1485

Tian L, Wang J, Zhou H, Wang J (2018) Automatic detection of forest fire disturbance based on dynamic modelling from MODIS time-series observations. Int J Remote Sens 39(12):3801–3815

Toschi I, Remondino F, Kellenberger T, Streilein A (2017) A survey of geomatics solutions for the rapid mapping of natural hazards. Photogramm Eng Remote Sens 83(12):843–859

Toschi I, Allocca M, Remondino F (2018) Geomatics mapping of natural hazards: overview and experiences. Int Archives Photogramm Remote Sens Spat Inf Sci 42(3/W4):505–512

Tucker CJ, Townshend JRG (2000) Strategies for monitoring tropical deforestation using satellite data. Int J Remote Sens 21(6):1461–1471

Vega SGD, de las Heras J, Moya D (2018) Post-fire regeneration and diversity response to burn severity in pinus halepensis Mill. forests. Forests 9:299. https://doi.org/10.3390/f9060299

Wallis R (1976) An approach to the space variant restoration and enhancement of images. In: Proc of Symposium on Current Mathematical Problems in Image Science, Monterey, CA

Wheeler D, Guzder-Williams B, Petersen R, Thau D (2018) Rapid MODIS-based detection of tree cover loss. Int J Appl Earth Obs Geoinf 69:78–87

Xu C, Manley B, Morgenroth J (2018) Evaluation of modelling approaches in predicting forest volume and stand age for small-scale plantations forests in New Zealand with RapidEye and LiDAR. Int J Appl Earth Observ Geoinf 73:386–396

Yu B, Chen F, Li B, Wang L, Wu M (2017) Fire risk prediction using remote sensed products: a case of Cambodia. Photogrammetric Engineering and Remote Sensing 83(1):19–25

Zhang L, Gruen A (2004) Automatic DSM generation from linear array imagery data. Int Archives Photogramm Remote Sens Spat Inf Sci 35(B3):128–133

Zhang L (2005) Automatic Digital Surface Model (DSM) Generation from Linear array Images. Ph.D. thesis, Institute of Geodesy and Photogrammetry, ETH Zurich, Switzerland, Mitteilungen Nr.88, p 219. ISBN 3-906467-55-4

Zhang L, Gruen A (2006) Multi-image matching for DSM generation from IKONOS imagery. ISPRS J Photogramm Remote Sens 60:195–211

Zhang L, Kocaman S, Akca D, Kornus W, Baltsavias E (2006) Test and performance evaluation of DMC images and new methods for their processing. In: Proceedings ISPRS commission I symposium, Paris, 3–6 Jul 2006

Zhang Y, Song C, Band LE, Sun G, Li J (2017) Reanalysis of global terrestrial vegetation trends from MODIS products: browning or greening? Remote Sens Environ 191:145–155